Article

Journal of Biomedical Nanotechnology
Vol. 14, 1277–1286, 2018
www.aspbs.com/jbn

In Vivo Dopamine Biosensor Based on Copper(I) Sulfide Functionalized Reduced Graphene Oxide Decorated Microelectrodes

Bowen Zhang[1,†], Changhui Li[1,2,†], Hang Zhang[1,†], Yun Chen[1], Hui Jiang[1], Leifeng Chen[1], Fawad Ur Rehman[1], and Xuemei Wang[1,*]

[1] *State Key Laboratory of Bioelectronics, National Demonstration Center for Experimental Biomedical Engineering Education, School of Biological Science and Medical Engineering, Southeast University, Nanjing 210096, China*
[2] *School of Chemistry and Chemical Engineering, Southeast University, Nanjing 211189, China*

A novel dopamine biosensor based on carbon fiber microelectrodes (CFMEs) modified with copper(I) sulfide functionalized nanocomposites of the reduced graphene oxide (Cu_2S/RGO) has been explored for the sensitive detection of dopamine and *in vivo* monitoring the neurotransmitters released by Drosophila's brain. The as-prepared Cu_2S/RGO decorated microelectrodes were characterized by scanning electron microscopy (SEM) and X-ray photoelectron spectroscopy (XPS), and cyclic voltammetry (CV). Our observations demonstrate that Cu_2S/RGO-CFMEs exhibited excellent catalytic activity and high selectivity for dopamine with relatively low detection limit (24 nM), wide linear range (i.e., from 0.1–20 μM) and outstanding reproducibility. Furthermore, the as-prepared new dopamine biosensor with high sensitivity and good stability was readily used to detect the amount of dopamine in the brain of drosophila, indicating the potential and promising application in the *in vivo* measurement of neurotransmitters without other electrochemical interference such as histidine, ascorbic acid, uric acid, and others.

KEYWORDS: *Dopamine, Microelectrode, Copper Sulfide, Reduced Graphene Oxide, Cyclic Voltammetry.*

INTRODUCTION

Microelectrodes are defined as electrodes with at least one dimension smaller than 25 μm.[1] The most common are platinum disk,[2] gold disk,[3] printed[4] and carbon fiber microelectrodes.[5] The small size of microelectrodes results in fast steady state electrochemical response, small ohmic losses, high sensitivity, low double-layer charging currents, etc.[1] Using scanning electrochemical microscopy (SECM) and differential pulse voltammetry (DPV),[6–8] microelectrodes have been widely applied for the detection of single cell and biopsy.[9–10] Carbon fiber microelectrodes (CFMES) have attracted much attention because of their small size (i.e., diameter of about 7 μm), low cost, chemical inertness, high temperature resistance and excellent electrical conductivity.[11–12] CFMEs have been modified by electrochemical deposition,[13] chemical adsorption,[14] physical adsorption and other methods,[15] which further enhanced their sensitivity and selectivity.

Since dopamine (DA, 4-(2-aminoethyl)benzene-1,2-diol) was first synthesized in the laboratory by the British scientists George Barger and James Ewens in 1910,[16–17] it was discovered that it is a key phenolic neurotransmitters in the hypothalamus and pituitary gland, which widely exists in the central nervous system, peripheral nervous system and kidney endocrine system of vertebrate and invertebrate.[18] As an important neurotransmitter, DA has been used as a drug for treating a variety of diseases.[19–20] Therefore, studies on the sensitive and selective determination of DA in the brain, blood, urine and tissues have an important practical significance both in the physiological research and in clinical applications.[21–22] Hitherto, most frequently-used methods to detect DA include ultraviolet absorption spectroscopy,[23] fluorescence,[24] high performance liquid chromatography (HPLC),[25] electrochemical determination,[26] etc. Since the catechol moiety

*Author to whom correspondence should be addressed.
Email: xuewang@seu.edu.cn
†These three authors contributed equally to this work.
Received: 2 December 2017
Accepted: 10 April 2018

of DA can be oxidized DA, it could be readily detected electrochemically.[27] In comparison to other detection techniques, the electrochemical detection has the advantages of high sensitivity, low cost, low detection limit, good selectivity, wide detection range and fast response, and the combination with microelectrodes makes it an appealing approach for the *in vivo* analysis.

Similar to carbon paste,[28] graphene, graphene oxide and reduced graphene oxide (RGO) have been widely used as platforms for electroanalysis.[29–31] In particular, RGO is advantageous as it has relatively high conductivity and, at the same time, still possesses chemical functionalities. It is beneficial to attach metal nanoparticles onto RGO as a means of assembling hybrid nanocomposites for sensing.[32–34] Cuprous(I) sulfide (Cu_2S) is a common sulfide with relatively high electrical conductivity, excellent thermal stability, good catalytic activity, low cost and readily available which can be easily applied to the fabrication of electrochemical sensor.[35–37] Herein, we combine the merits of RGO with that of Cu_2S for obtaining a highly sensitive and selective electrochemical sensor for DA based on the nanostructured interface of Cu_2S/RGO nanocomposites. Moreover, the special structure of RGO with oxygen-containing functional groups enabled modification of CFMEs with the as-prepared Cu_2S nanocomposites to form a novel DA electrochemical sensor applied for the *in vivo* monitoring DA of *drosophila melanogaster*.

MATERIALS AND METHODS

Materials

Graphene oxide was purchased from XF NANO, Inc. (China). DA, ascorbic acid (AA), histidine (His), uric acid (UA), β-D(+)-glucose (GLU) and chitosan were obtained from Sigma Co. Na_2S, $CuCl_2$, polyethylene benzene sulfonic acid sodium and hydrazine hydrate were also purchased from Sigma Co. All other chemicals were of analytical grade and used as received without any further purification. A physiological PBS solution containing KH_2PO_4 (2 mM), Na_2HPO_4 (10 mM), NaCl (136 mM), and KCl (2 mM) was prepared immediately before experiments. All the solutions were prepared by doubly-deionized distilled water. *Drosophila melanogaster* was obtained from the Institute of Life Sciences, Southeast University.

Preparation of CFMEs

CFMEs were prepared as described previously where a carbon fiber was used as the electrode material.[12] Specifically, a cluster of carbon fiber (7 μm in diameter) was cut into a short piece before cleaned by ultrasonic with acetone, ethanol and doubly-deionized distilled water successively to dissolve the attachments on the surface and then dried thoroughly in the oven at 80 °C. A copper wire (about 12 cm) was inserted into a glass capillary (length: 10 cm, inter diameter: 0.5 mm) leaving a 2 cm length of copper wire outside. A single carbon fiber was attached to one end of the copper wire with a conductive silver adhesive. After it had been dried, the carbon fiber was moved into the middle of the glass capillary and then the capillary was pulled to expose the carbon fiber out through a tip diameter about 9 μm. Then, the microelectrodes tip was vertically immersed into paraffin, which was melted in an 80 °C water-bath for 30 s. During this process, the paraffin entered into the gap between the carbon fiber and the glass on the tip because of capillary forces. After the paraffin cooled, the microelectrode was cleaned by dipping in acetone for about 30 s to get rid of the paraffin adsorption on the carbon fiber surface. The etching process was performed in a 1 M NaOH solution by using a double potential step of $\pm$2 V with a uniform step time of 0.01 s. A control console was used to fix the capillary and control the vertical position of the tip in order to control accurately the length of the carbon fiber (50 μm in our experiment).

Synthesis of Cu_2S/RGO Nanocomposites

Graphene oxide (10 mg), polyethylene benzene sulfonic acid sodium (20 mg) and $CuCl_2$ solution (50 μL 1 M) were dispersed in 30 mL doubly-deionized distilled water with ultrasonic treatment for 30 min, and then an aliquot of freshly prepared Na_2S solution (50 μL 1 M) was gradually added with stirring for 10 min. Hydrazine hydrate (100 μL) was added with stirring for 1 hour under protection of nitrogen gas, respectively. The as-obtained mixture was transferred into a high pressure autoclave, and was heated at 230 °C for 3 hours. After the reaction was completed, the mixture was washed several times and dispersed into 0.01% chitosan solution developing black suspension of 2 mg/mL and stored at 4 °C.

Preparation of Cu_2S/RGO-CFMEs

The CFMEs pretreatment were performed in a 0.1 M sulfuric acid solution by applying cyclic voltammetry in the potential range from $-$0.4 V to +0.7 V at a scan rate of 10 mV/s until a stable cyclic voltammogram was obtained. The electrochemical performances of the electrodes were initially evaluated by cyclic voltammetry in potassium hexacyanoferrate(III) solution, which showed an ideal s-shape. Then, the microelectrode was fixed to a translation stage, and 5 μL of the as-prepared Cu_2S/RGO suspension was dropped on a hydrophobic polyethylene surface. Finally, the microelectrode was inserted into the droplet of Cu_2S/RGO suspension accurately by controlling the translation stage. Consequently, Cu_2S/RGO was attached to the CFME by physical adsorption forming Cu_2S/RGO-CFME.[38–39]

Drosophila Experiments

The drosophila under good conditions was raised for 3 days shielded from light prior to the dissection. The skulls of the drosophila were stripped by tweezers under

the stereoscopic microscope to ensure the accurate position of the working electrode. Then, the drosophila was fixed on an ITO electrode with PBS solution as the electrolyte, and the as-prepared microelectrode was accurately moved to the top of the brain by 3D operation console. After the samples were illuminated under a low light for at least 1 hour, the three-electrode system employing Cu_2S/RGO-CFMEs as working electrode, an Ag/AgCl as reference electrode and the ITO electrode as counter electrode was used in PBS solution as a background and move down the microelectrode accurately inserting the gap of *drosophila's* brain to detect DA by voltammetry by scanning from −0.4 to +1 V at rate of 100 V/s, and then high-power red light (615–635 nm, LED) was used to stimulate the drosophila.

Characterization of Cu_2S/RGO-CFMEs

Surface Morphology

The surface morphology and relevant microstructure of the nanocomposites modified microelectrodes were characterized by scanning electron microscope (SEM; Zeiss, Germany). To prepare the SEM samples, a Cu_2S/RGO-CFME was fabricated and subsequently dried slowly in air and then examined under SEM.

XPS Analysis

The valence state of materials was determined by X-ray photoelectron spectroscopy (XPS; Ulvac-Phi, Japan). The potential was ranged from 0–1100 eV.

Electrochemical Measurements

All electrochemical measurements were performed by using a modular electrochemical system Autolab PGSTAT302N (Eco Chemie, Netherlands) driven by NOVA 1.10 software (Eco Chemie). The three-electrode system includes an Ag/AgCl electrode as the reference electrode, a Pt wire or ITO electrode as the counter electrode and the as-prepared Cu_2S/RGO-CFMEs or CFMEs as the working electrode. The electrochemical measurements were performed in N_2-saturated solution at room temperature (ca. 20 °C).

RESULTS AND DISCUSSION

Surface Morphology and Microstructure

The SEM images illustrate the general morphology of Cu_2S/RGO, CFMEs and Cu_2S/RGO-CFMEs. From Figure 1(a), it is observed that the Cu_2S nanoparticles cover, and are quite well distributed on the entire graphene oxide surface to form a Cu_2S/RGO nanocomposite. The length of the microelectrode was controlled by electrochemical etching. Cu_2S/RGO nanocomposite is attached onto the surface of CFMEs by physical absorption to form Cu_2S/RGO-CFMEs. The SEM imaging of CFMEs shows that the length was about 50 μm and the diameter was about 7 μm (Fig. 1(b)). The length of Cu_2S/RGO-CFMEs was equal to CFMEs and the diameter was about 8 μm (Fig. 1(c)). Furthermore, the XPS study confirmed the valence states and the composition of nanocomposites. The survey scan XPS spectrum of the nanocomposites in Figure 2(a) confirms the presence of C, O, Cu and S on the surface. Figure 2(b) shows the XPS C1*s* deconvolved into three peaks: C–C/C=C (284.5 eV), C–O (286.2 eV) and C = O–O (287.8 eV), respectively. This confirms that the carbon nanomaterials in the composites is RGO.[40–41] Figures 2(c), (d) are high resolution XPS images of Cu 2*p* and S 2*p*. There are two different binding energy peaks located at 952.5 eV and 932.38 eV representing Cu $2p_{1/2}$ and Cu $2p_{3/2}$, respectively, and no "shake-up" peaks were found in the higher binding energy spectrum (Fig. 2(c)), which demonstrates that the copper in the nanocomposites only presents in the +1 valence state.[38, 42–45] Moreover, the binding energy peaks of S $2p_{1/2}$ and S $2p_{3/2}$ are 163.5 eV and 162 eV, respectively, and there are no other peaks, indicating that only Cu and S constitute the Cu_2S.[46–48] Therefore, the SEM and XPS results verify that Cu_2S/RGO nanocomposites have been successfully synthesized.

Cyclic Voltammetry of DA at CFMEs and Cu_2S/RGO-CFMEs

The cyclic voltammetry (CV) with a low scan rate of 10 mV/s was utilized to characterize the relevant CFMEs and Cu_2S/RGO-CFMEs. It can be seen (Figs. 3(a, b)) that both microelectrodes show a clear electrochemical response to DA in PBS solution. However, they also exhibit catalytic activity towards AA (Figs. 3(c, d)) at a similar potential, resulting in a major interference for detecting DA *in vivo*. Thus, it was better to use CV with higher scan rates for the detection of neurotransmitters. Figure 4(a) shows the background-subtracted CV curves of CFMEs and Cu_2S/RGO-CFMEs for 5 μM DA scanning across a potential range of −0.4 to +1.0 V and back at

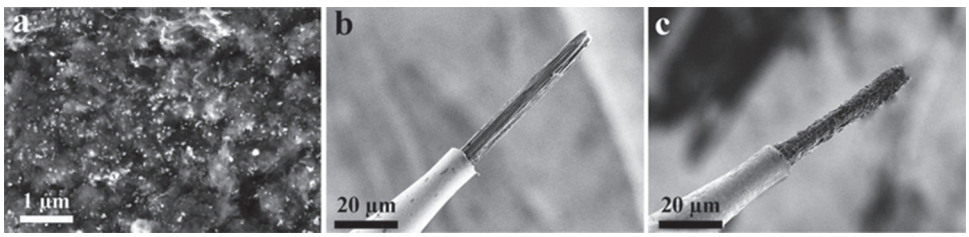

Figure 1. SEM images of (a) Cu_2S/RGO; (b) CFMEs; (c) Cu_2S/RGO-CFMEs.

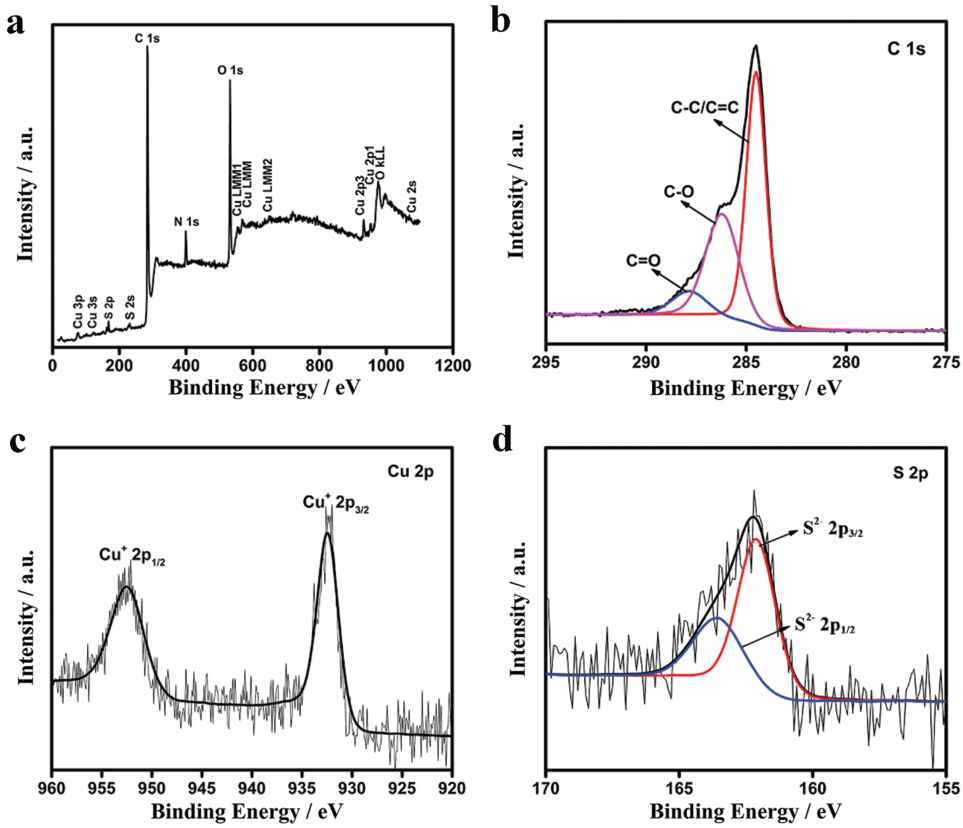

Figure 2. **(a) Survey scan XPS spectrum of Cu_2S/RGO; Narrow spectra of (b) C 1*s*; (c) Cu 2*p*; (d) S 2*p*.**

100 V/s in PBS solution. The two types of electrodes had good electrochemical response towards DA, which was oxidized and then reduced on the surface of electrodes forming a pair of redox peaks.[49] As compared with bare CFMEs, Cu_2S/RGO-CFMEs had a bigger current response for DA with a narrower peak width, in that Cu_2S/RGO-CFMEs had good electrochemical catalytic effects for DA due to larger surface area and better electrical conductivity. The shoulder peak around 0.55 V could be attributed to the reduction of copper(I). The illustration shows that the average ΔE_p (i.e., ΔE_{pk} refers to the potential difference between anodic and cathodic peaks) for Cu_2S/RGO-CFMEs were significantly smaller than those for CFMEs ($n = 5$ each, $p < 0.01$, t-test) implies decreased overpotential of Cu_2S/RGO-CFMEs for DA.[8]

The apparently different ΔE_{pk} and peak currents could be due to different components and nanostructured geometries between the Cu_2S/RGO-CFMEs and CFMEs with different catalytic activity, diffusion and adsorptive behavior to DA. Alternatively, Cu_2S/RGO-CFMEs with lower ΔE_p and much bigger peak currents may be associated with the effective adsorption of metal compounds and some functional groups on the surface of electrodes, which greatly enhanced the electron transfer efficiency and catalytic activity of the electrode.[50]

The fast scanning CV study was utilized to further investigate the charge transport characteristics of the Cu_2S/RGO-CFMEs at different scan rates from 10–200 V/s. Figure 4(b) displays that with the increase of scanning rates both anodic ($i_{pk,a}$) and cathodic peak currents ($i_{pk,c}$) increase. In addition, the ΔE_{pk} significantly increases while the scanning rate is greater than 100 V/s. The illustration shows that $i_{pk,a}$ and $i_{pk,c}$ had a good linearity with the scan rate with correlation coefficients R^2 of 0.992 and 0.993, respectively, indicating that the electrochemical behavior of Cu_2S/RGO-CFMEs for DA is mainly controlled by adsorption.

Cyclic Voltammetry Response to DA Detection

The CV study was further exploited to evaluate the electrocatalytic activity of CFMEs and Cu_2S/RGO-CFMEs for detection of different concentrations of DA at a scan rate of 100 V/s (Fig. 5). Figure 6(a) shows the background-subtracted CVs of CFMEs for 2–200 μM DA. It indicates that the peak currents *ip, a* and *ip, c* increase with DA concentration, while the cathodic peak potential ($E_{pk,c}$) and anodic peak potential ($E_{pk,a}$) slightly shift at higher concentrations. The CVs of Cu_2S/RGO-CFMEs for different concentrations of DA is shown in Figure 6(b). The peak currents increase with the DA concentration, but the sensitivity of electrode for DA declined gradually.

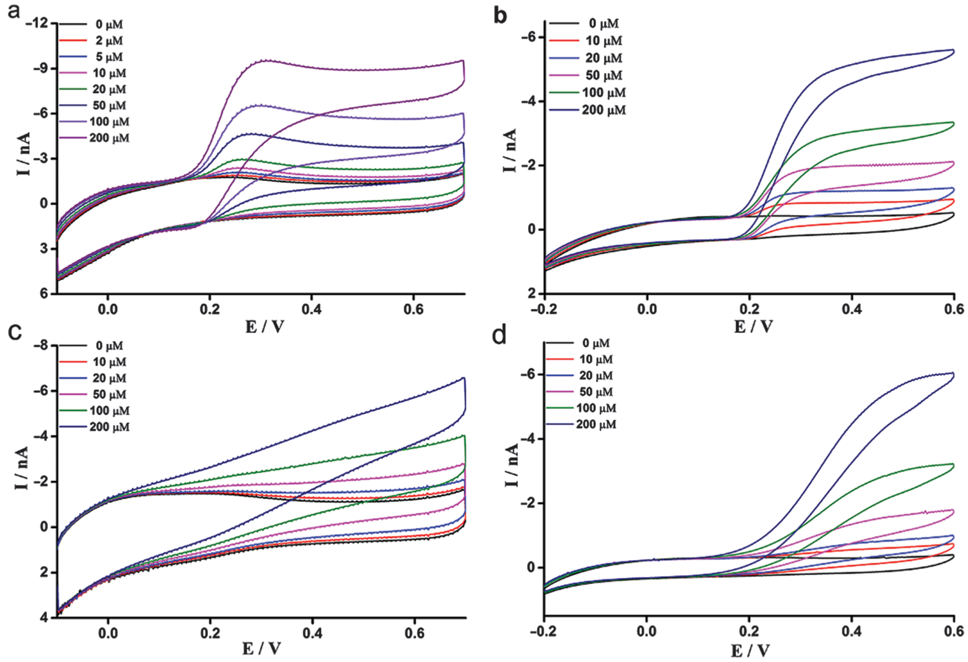

Figure 3. CVs of Cu_2S/RGO-CFMEs in the absence and presence of different concentrations of DA (a) and AA (c) at voltage range of −0.1 to +0.7 V, and CVs of CFMEs in the absence and presence of different concentrations of DA (b) and AA (d) at voltage range of −0.2 to +0.6 V, with scan rate of 50 mV/s in N2-saturated PBS solution.

Figure 6(c) shows the corresponding calibration curve for CFMEs, indicating that $i_{pk,a}$ and $i_{pk,c}$ have good linear relationship with DA concentration in the range of 2–200 μM. The linear regression equations for the peak currents are t $i_{pk,a}$ (μA) $= 8.365 \times 10^{-4}$C $+ 0.006024$ with a correlation coefficient of $R^2 = 0.993$ and a sensitivity of 0.735 ± 0.005 pA/(μM μm^2), and $i_{pk,c}$(μA) $= 4.965 \times 10^{-4}$C $+ 0.00716$ (where C is the concentration of DA, $n =$ 3 electrodes) with a correlation coefficient of $R^2 = 0.993$ and a sensitivity of 0.436 ± 0.004 pA/(μM μm^2). As shown in Figure 6(d), $i_{pk,a}$ and $i_{pk,c}$ of Cu_2S/RGO-CFMEs for DA have good linearity with DA concentration in the range of 0.1–20 μM. The linear regression equations for the peak currents is $i_{pk,a}$(μA) $= 0.0292$C $+ .0331$ with a correlation coefficient of $R^2 = 0.996$ and a sensitivity of 22.34 ± 0.18 pA/(μMμm^2), and $i_{pk,c}$(μA) $= 0.0225$C $+ 0.022$ (where C is the concentration of DA, $n = 3$ electrodes) with a correlation coefficient of $R^2 = 0.996$ and a sensitivity of 17.22 ± 0.13 pA/(μM μm^2). The sensitivity of Cu_2S/RGO-CFMEs for DA decreases gradually when the concentration of DA becomes greater than 20 μM, which may be due to the fact that the redox of DA on the electrode surface is due to an adsorption-controlled process. The results indicate that the cathodic peak width is narrower than the anodic counterpart

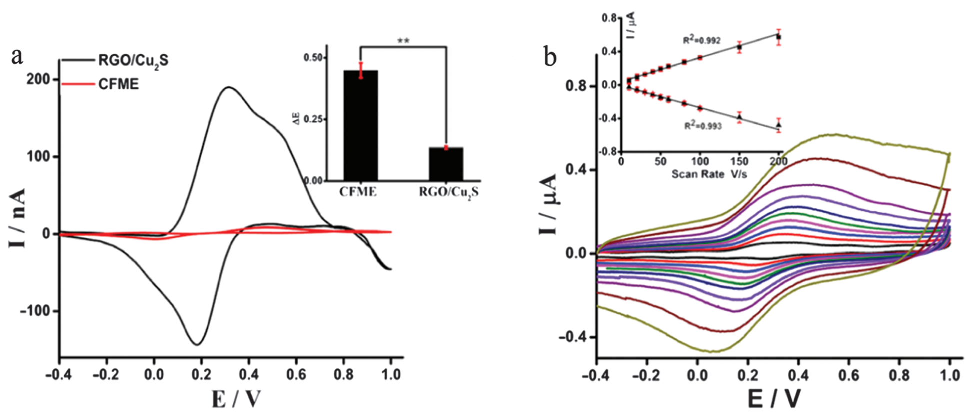

Figure 4. (a) Background-subtracted CV of 5 μM DA using CFMEs (red line) and Cu_2S/RGO-CFMEs (black line). Inset: The ΔE_p values of the electrodes are significantly different ($n = 5$ each, $p < 0.01$, t-test). All electrodes were scanned from −0.4 to +1.0 V and back at 100 V/s in PBS solution; (b) CV of Cu_2S/RGO-CFMEs in PBS at 10, 20, 30, 40, 50, 60, 80, 100, 150 and 200 V/s. The inset shows the dependence of the anodic and cathodic peak currents on scan rates.

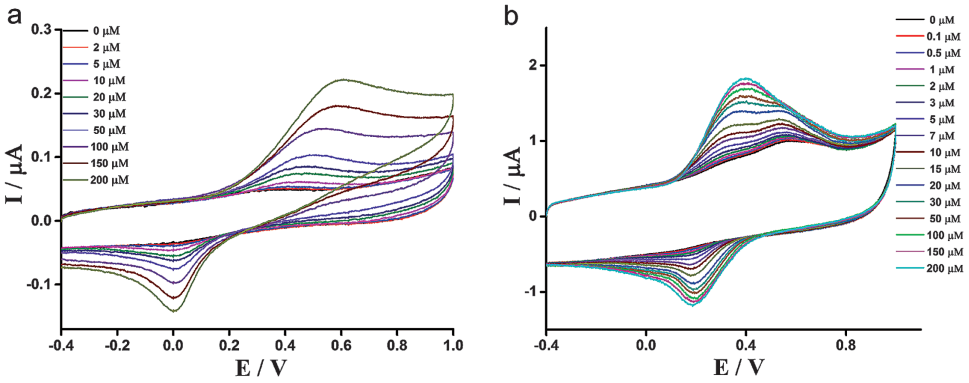

Figure 5. **CVs of CFMEs and Cu_2S/RGO-CFMEs in the absence and presence of different concentrations of DA in N2-saturated PBS solution. Voltage range of −0.4 to +1 V and scan rate: 100 V/s.**

and $E_{pk,c}$ is more stable than the anodic peak potential than $\varphi p, a$. Consequently, a novel DA electrochemical biosensor based on Cu_2S/RGO-CFMEs with lower detection limit and higher sensitivity than CFMEs seems better in detecting DA *in vivo*.

Anti-Interference Ability and Stability of Microelectrodes

The good selectivity and stability was one of the most important indexes to measure the performance of electrochemical biosensor, and CVs was applied to research the interference of other electrochemical active substances in the process of CFMEs and Cu_2S/RGO-CFMEs for detection of DA. AA, a kind of anionic antioxidants, has a significantly higher level than DA in the brain,[51–52] but with a similar redox potential to DA. Histidine (His) is a neurotransmitter that regulates sleep.[53] Although other common biomolecules, such as glucose and uric acid, are also common electrochemical active substances in the organism, they have less effect on the electrochemical detection of DA (Fig. 7). Generally, AA and His show certain influence on the detection of DA.

Table I shows the relevant mean and standard deviations of $i_{pk,a}$, $E_{pk,a}$, $i_{pk,c}$ and $E_{pk,c}$ c determined in

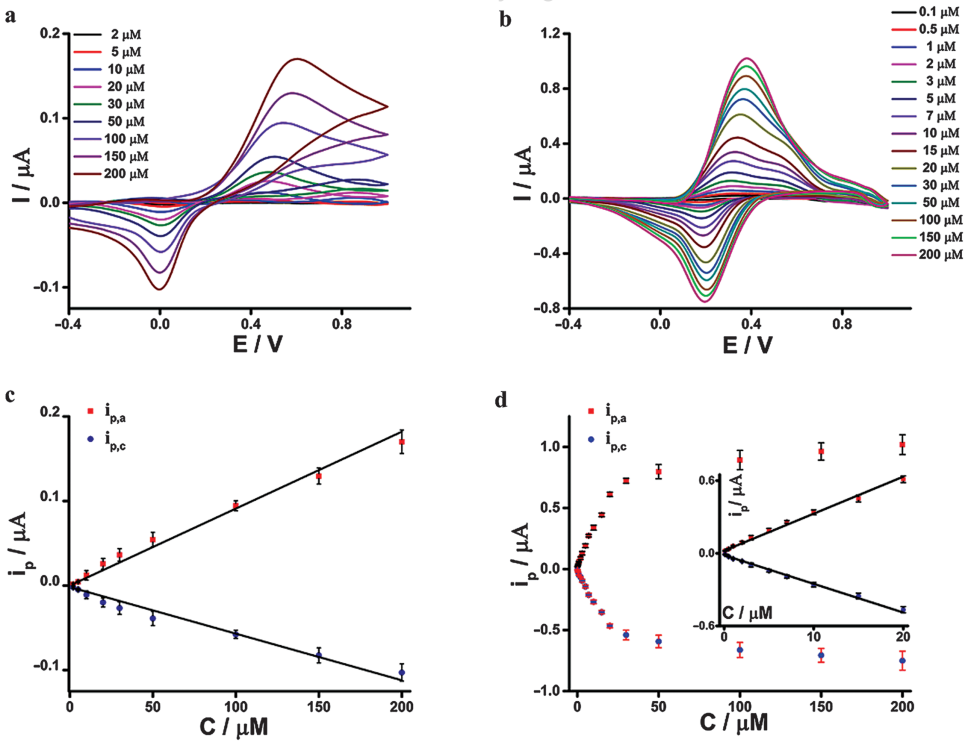

Figure 6. **Background-subtracted CV of (a) CFMEs; (b) Cu_2S/RGO-CFMEs in the presence of different concentrations of DA with scan rate of 100 V/s. Plots of normalized peak currents as a function of DA concentration for (c) CFMEs; (d) Cu_2S/RGO-CFMEs. ($n = 3$ electrodes).**

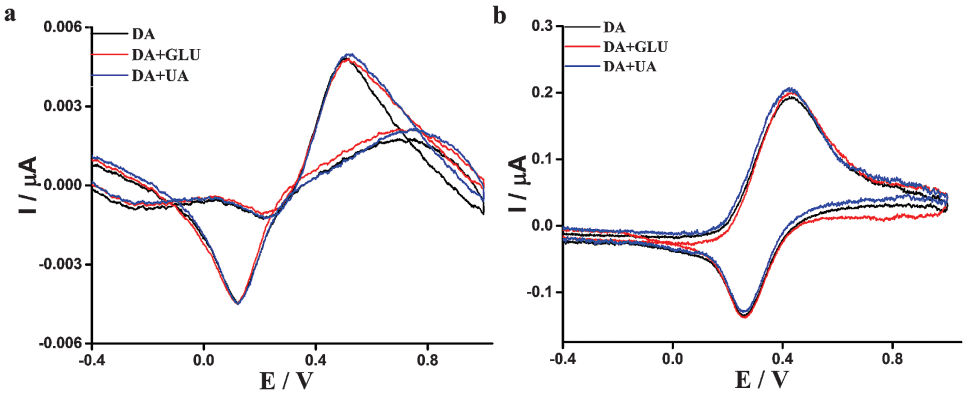

Figure 7. **Background-subtracted CVs of (a) CFMEs, (b) Cu_2S/RGO-CFMEs in the presence of 5 μM DA (black line), mixture of 5 μM DA and 1 mM GLU (red line), and mixture of 5 μM DA and 20 μM UA (blue line).**

this study. The changes of $i_{pk,a}$, $E_{pk,a}$, $i_{pk,c}$ and $E_{pk,c}$ (derived from the background-subtracted CV) of CFMEs and Cu_2S/RGO-CFME under different substrates indicate that both AA and His have extremely significant impacts on the peak currents and potentials at CFMEs for DA detection (one-way ANOVA, LSD post-test, $p < 0.01$, $n = 3$), which limited its further application for the *in vivo* detection of DA (Fig. 7), while the average of $i_{pk,a}$ and $E_{pk,a}$ for 5 μM DA at Cu_2S/RGO-CFMEs shows significantly difference as compared with the mixture of 5 μM DA and 20 μM AA by using the same electrodes (paired post-test, $p < 0.01$). The average $i_{pk,c}$ and $E_{pk,c}$ for DA at Cu_2S/RGO-CFMEs is different from those for the mixture of DA and AA, however, the difference was not significant (unpaired post-test, $i_{pk,c}$ $p = 0.424$; $E_{pk,c}$ $p = 0.106$). The average of $i_{pk,a}$ for DA at Cu_2S/RGO-CFMEs is significantly smaller than that for the mixture of DA and His by using the same electrodes (paired post-test, $p < 0.01$), and the difference between DA and mixture of DA and His for $E_{pk,a}$ $i_{pk,c}$ and $E_{pk,c}$ are not significant (unpaired post-test, $E_{pk,a}$ $p = 0.283$; $i_{pk,c}$ $p = 0.219$; $E_{pk,c}$ $p = 0.058$). This observation indicates that AA and His have significant interference on the anodic peak of DA by using Cu_2S/RGO-CFMEs while minor interference on the cathodic peak. Consequently, the Cu_2S/RGO-CFMEs sensor with excellent selectivity and sensitivity has practical value and good application prospects.

The tests of reproducibility and storage stability of the microelectrode are very important for *in vivo* measurements.[54] Microelectrodes were typically used *in vivo* for hours at a time to measure electrochemical active substances. Therefore, the relevant electrodes must have a stable electrochemical response for several hours.[55] According to the anti-interference studies described above, $i_{pk,c}$ of DA at Cu_2S/RGO-CFMEs was hardly affected by other electrochemical active substances. This important parameter was used to assess the stability of the microelectrode. As shown in Figure 8(c), the CFMEs' sensitivity gradually decreased over time and dropped to 50.5% of the original current after 3 h. Conversely, the sensitivity at Cu_2S/RGO-CFMEs slightly declined to 95.6 ± 4.0% of its initial response sensitivity within 5 hours, indicating a relatively long-term stability and good reproducibility. Therefore, all of these studies imply that Cu_2S/RGO nanocomposites modified CFMEs were significantly superior to CFMEs for detection of DA, which have excellent selectivity and sensitivity for the relevant *in vivo* study of some biological process.

In Vivo Detection of DA Through Cu_2S/RGO-CFMEs

It is reported that the detection of DA *in vivo* can be realized by using genetic mutation or gene modified light sensitive larvae as experimental samples, because the ventral

Table I. **Average electrochemical parameters of Figures 8(a), (b).**

		$i_{pk,a}$ (nA)	$E_{pk,a}$ (V)	$i_{pk,c}$ (nA)	$E_{pk,c}$ (V)
CFMEs	DA	4.55 ± 0.04	0.44 ± 0.01	4.52 ± 0.1	0.01 ± 0.01
CFMEs	DA+AA	5.95 ± 0.11[a]	0.48 ± 0.02[a]	1.85 ± 0.14[a]	0.07 ± 0.02[a]
CFMEs	DA+His	5.31 ± 0.11[b]	0.53 ± 0.03[b]	3.64 ± 0.11[b]	−0.01 ± 0.01[b]
Cu_2S/RGO-CFMEs	DA	189.67 ± 1.53	0.32 ± 0.01	140.33 ± 2.52	0.18 ± 0.01
Cu_2S/RGO-CFMEs	DA+AA	174.67 ± 4.51[a]	0.40 ± 0.02[a]	135.33 ± 9.50	0.20 ± 0.02
Cu_2S/RGO-CFMEs	DA+His	261.00 ± 7.01[b]	0.31 ± 0.01	148.33 ± 7.50	0.16 ± 0.01

Notes: All $n = 3$ electrodes. It is evident that the relevant electrochemical parameters of Figures 8(a), (b) for detection of mixtures of 5 μM DA and 20 μM AA and mixtures of 5 μM DA and 5 μM His are significantly different than for 5 μM DA at the same microelectrodes ($p < 0.01$).

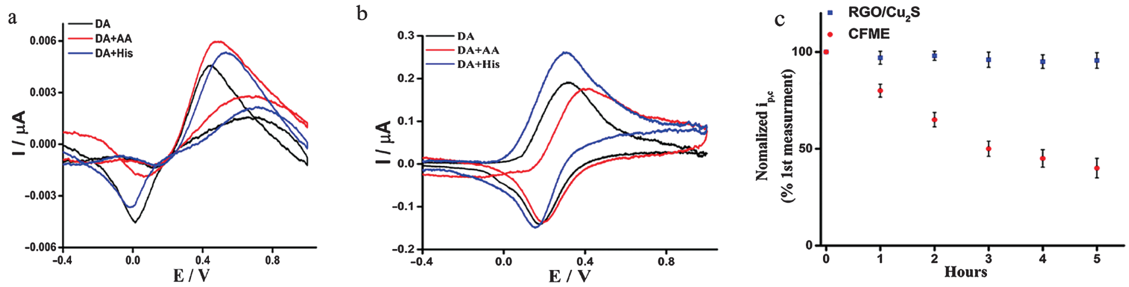

Figure 8. Background-subtracted CV of (a) CFMEs; (b) Cu_2S/RGO-CFMEs in the presence of 5 μM DA (black line), mixture of 5 μM DA and 20 μM AA (red line), and mixture of 5 μM DA and 5 μM His (blue line); (c) Stability experiment was performed by testing the response of CFMEs (red) and Cu_2S/RGO-CFMEs (blue) to 5 μM DA every 1 h for 5 h ($n = 3$ electrodes).

nerve cord can release DA under the stimulation of light with specific wavelengths (such as red light[8] and blue light[56]). On the basis of the above observations, the relevant electrochemical detection has been further exploited *in vivo* by using the novel Cu_2S/RGO-CFMEs to qualitatively detect DA in drosophila's brain. The CV has the characteristic anodic and cathodic peaks for electrochemically active substances in drosophila's brain (Fig. 9). The corresponding currents are significantly increased under red light stimulation, while the peak potential has almost no shift. The illustration shows that the relevant $E_{pk,a}$ mean value of 0.45 V was significantly higher than the mean value of detection of DA in buffer solution (0.32 V) ($n = 6$ each, $p < 0.01$, t-test). According to the anti-interference study, a reasonable explanation for the change in $E_{pk,a}$ would be the effects of other electrochemically active substances in the brain disturbance. The average value of $E_{pk,c}$ was 0.16 V, which was similar to that in the detection of DA in solution (unpaired t-test, $p = 0.326$, $n = 6$ each). It is evident that the cathodic peaks originated only from the successive reduction after oxidation of DA. Conversely, the concentration of DA was also calculated by $i_{pk,c}$ through the DA electrochemical sensor based on Cu_2S/RGO-CFMEs for the relevant quantitative *in vivo* detection of some specific biological process.

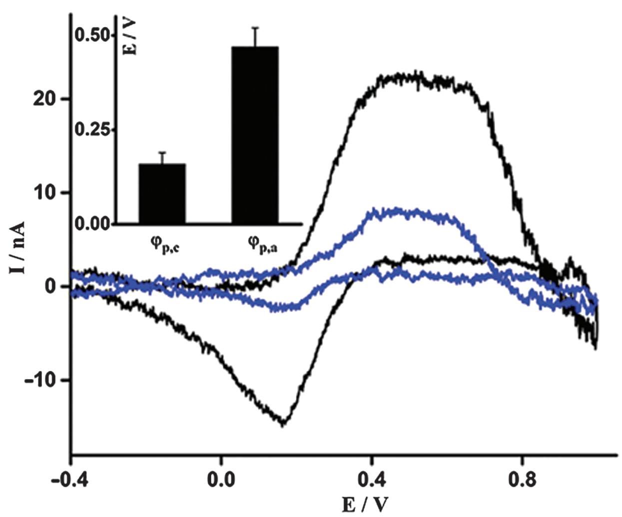

Figure 9. Background-subtracted CV of DA *in vivo* using Cu_2S/RGO-CFMEs at low light conditions (blue line) and stimulation of red light (black line). Inset: Corresponding values of $E_{pk,c}$ and $E_{pk,a}$. Error bars are the standard error of the mean ($n = 6$ electrodes).

CONCLUSIONS

In summary, in this study we fabricated a novel DA sensor constructed on the basis of Cu_2S/RGO nanocomposites modified carbon fibers' microelectrode (Cu_2S/RGO-CFMEs). The electrochemical performance of the as-prepared sensor was assessed by using cyclic voltammetry, which demonstrate that the Cu_2S/RGO-CFMEs as a new DA electrochemical sensor have excellent selectivity, stability and sensitivity, with a marvelous linear range from 0.1 μM to 20 μM, and a low detection limit of 24 nM. The modified microelectrode has the advantages of reducing tissue damage and can readily improve the spatial resolution for the *in vivo* DA detection. It is evident that the Cu_2S/RGO-CFMEs could have potential applications in the *in vivo* measurements of neurotransmitters in that it can avoid the interference of other components like histidine, ascorbic acid, uric acid, and others.

Acknowledgments: This work was supported by National Key Research and Development Program of China (2017YFA0205300), National Natural Science Foundation of China (91753106, 21327902, 81325011 and 21675023).

REFERENCES

1. D. T. X. Nguyen, T. B. Tran, P. D. Nguyen, and J. Mi, Addressing of LnCaP cell using magnetic particles assisted impedimetric microelectrode. *J. Nanosci. Nanotechnol.* 16, 2933 (**2016**).
2. T. Sun, B. Y. Yu, and B. J. Zacher, Scanning electrochemical microscopy of individual catalytic nanoparticles. *Angew. Chem. Int. Ed. Engl.* 53, 14120 (**2014**).
3. H. S. Ahn and A. J. Bard, Surface interrogation of CoPi water oxidation catalyst by scanning electrochemical microscopy. *J. Am. Chem. Soc.* 137, 612 (**2015**).
4. T. S. Safaei, J. Das, S. S. Mahshid, P. M. Aldridge, E. H. Sargent, and S. O. Kelley, Image-reversal soft lithography: Fabrication of

ultrasensitive biomolecular detectors. *Adv. Healthc. Mater.* 5, 893 **(2016)**.
5. E. C. Mitchell, L. E. Dunaway, G. S. McCarty, and L. A. Sombers, Spectroelectrochemical characterization of the dynamic carbon-fiber surface in response to electrochemical conditioning. *Langmuir* 33, 7838 **(2017)**.
6. F. P. Filice, M. S. Li, J. D. Henderson, and Z. Ding, Mapping Cd(2)(+)-induced membrane permeability changes of single live cells by means of scanning electrochemical microscopy. *Anal. Chim. Acta* 908, 85 **(2016)**.
7. S. Bergner, P. Vatsyayan, and F. M. Matysik, Recent advances in high resolution scanning electrochemical microscopy of living cells—A review. *Anal. Chim. Acta* 775, 1 **(2013)**.
8. F. F. Wang, W. Wang, X. He, L. H. Han, J. Z. Zhou, Z. Q. Tian, Z. W. Tian, and D. P. Zhan, Nanofabrication of the gold scanning probe for the STM-SECM coupling system with nanoscale spatial resolution. *Sci. China Chem*. 60, 649 **(2017)**.
9. J. Zhou, D. Jiang, and H. Y. Chen, Nanoelectrochemical architectures for high-spatial-resolution single cell analysis. *Sci. China Chem*. 60, 1277 **(2017)**.
10. C. Yang, E. Trikantzopoulos, C. B. Jacobs, and B. J. Venton, Evaluation of carbon nanotube fiber microelectrodes for neurotransmitter detection: Correlation of electrochemical performance and surface properties. *Anal. Chim. Acta* 965, 1 **(2017)**.
11. Y. Y. Zhang, X. Y. Bai, X. M. Wang, K. K. Shiu, Y. L. Zhu, and H. Jiang, Highly sensitive graphene–Pt nanocomposites amperometric biosensor and its application in living cell H_2O_2 detection. *Anal. Chem*. 86, 9459 **(2014)**.
12. C. Ma, J. Sheng, Y. Zhao, R. R. Wang, H. X. Zhang, and J. L. Shi, Preparation and comparative study of microporous and mesoporous carbon nanofibers as supercapacitor electrodes. *J. Nanosci. Nanotechnol.* 18, 699 **(2018)**.
13. Y. Chen, Q. W. Li, H. Jiang, and X. M. Wang, Pt modified carbon fiber microelectrode for electrochemically catalytic reduction of hydrogen peroxide and its application in living cell H_2O_2 detection. *J. Electroanal. Chem*. 781, 233 **(2016)**.
14. H. Y. Liu, C. C. Gu, C. Hou, Z. Z. Yin, K. Fan, and M. Z. Zhang, Plasma-assisted synthesis of carbon fibers/ZnO core–shell hybrids on carbon fiber templates for detection of ascorbic acid and uric acid. *Sensors and Actuators B: Chem*. 224, 857 **(2016)**.
15. N. R. Ferreira, A. Ledo, J. G. Frade, G. A. Gerhardt, J. Laranjinha, and R. M. Barbosa, Electrochemical measurement of endogenously produced nitric oxide in brain slices using nafion/O-phenylenediamine modified carbon fiber microelectrodes. *Anal. Chim. Acta* 535, 1 **(2005)**.
16. S. R. Hu, Q. T. Huang, Y. Lin, C. Wei, H. Q. Zhang, W. X. Zhang, Z. B. Guo, X. X. Bao, J. G. Shi, and A. Y. Hao, Reduced graphene oxide-carbon dots composite as an enhanced material for electrochemical determination of dopamine. *Electrochim. Acta* 130, 805 **(2014)**.
17. C. Y. Jiang, X. Z. Zeng, B. J. Wu, Q. Zeng, W. H. Pang, and J. Tang, Electrochemical co-deposition of reduced graphene oxide-gold nanocomposite on an ITO substrate and its application in the detection of dopamine. *Sci. China Chem*. 60, 151 **(2017)**.
18. A. Roychoudhury, S. Basu, and S. K. Jha, Dopamine biosensor based on surface functionalized nanostructured nickel oxide platform. *Biosens. Bioelectron*. 84, 72 **(2016)**.
19. Y. Niv, Neuroscience: Dopamine Ramps Up. *Nature* 500, 533 **(2013)**.
20. H. T. Yang, X. Y. Zhao, H. B. Chang, R. M. Xing, J. H. Yang, S. H. Liu, and X. H. Liu, Sensitive determination of dopamine and paracetamol based on carbon nanotubes-supported Pd nanoparticles. *J. Nanosci. Nanotechnol*. 18, 500 **(2018)**.
21. J. H. An, B. K. Oh, and J. W. CHoi, Detection of tyrosine hydroxylase in dopaminergic neuron cell using gold nanoparticles-based barcode DNA. *J. Biomed. Nanotechnol.* 9, 639 **(2013)**.
22. M. Marinelli and J. E. McCutcheon, Heterogeneity of dopamine neuron activity across traits and states. *Neuroscience* 282, 176 **(2014)**.
23. W. J. Barreto, S. R. Barreto, R. A. Ando, P. S. Santos, E. DiMauro, T. Jorge, and I. R. Raman, UV-Vis and EPR characterization of two copper dioxolene complexes derived from L-dopa and dopamine. *Spectrochimica Acta Part A: Molecular Spectroscopy* 71, 1419 **(2008)**.
24. L. Zhang, H. Jiang, M. Selke, and X. M. Wang, Selective cytotoxicity effect of cerium oxide nanoparticles under UV irradiation. *J. Biomed. Nanotechnol*. 10, 278 **(2014)**.
25. A. Vadivaambigai, P. A. Senthilvasan, N. Kothurkar, and M. Rangarajan, Graphene-oxide-based electrochemical sensor for salicylic acid. *Nanosci. Nanotechnol. Lett*. 7, 140 **(2015)**.
26. Q. W. Lian, Z. F. He, Q. He, A. Luo, K. W. Yan, D. X. Zhang, X. Q. Lu, and X. B. Zhou, Simultaneous determination of ascorbic acid, dopamine and uric acid based on tryptophan functionalized graphene. *Anal. Chim. Acta* 823, 32 **(2014)**.
27. J. Cheng, R. Zhong, W. Wan, H. Li, and J. Zhu, Amino acid detection from the leaves of camellia nitidissima chi using novel husk-derived graphene nanoshuttles. *Nanosci. Nanotechnol. Lett*. 9, 1742 **(2017)**.
28. Y. Liu, K. Liu, H. Dong, L. Zhang, Y. Deng, C. Ma, and Z. Wang, Acetylcholinesterase biosensor for carbaryl detection based on nanoporous pseudo carbon paste electrode. *Nanosci. Nanotechnol. Lett*. 8, 785 **(2016)**.
29. C. H. Li, X. L. Liu, Y. Y. Zhang, Y. Chen, T. Y. Du, H. Jiang, and X. M. Wang, A novel nonenzymatic biosensor for evaluation of oxidative stress based on nanocomposites of graphene blended with CuI. *Anal. Chim. Acta* 933, 66 **(2016)**.
30. Z. Zhu, Y. T. Guo, T. C. Chang, R. J. Wu, and W. D. Lin, Enhanced humidity-sensitive properties of novel graphene/zinc oxide nanocomposite films. *Nanosci. Nanotechnol. Lett*. 10, 46 **(2018)**.
31. D. J. Park, J. H. Choi, W. J. Lee, S. H. Um, and B. K. Oh, Selective electrochemical detection of dopamine using reduced graphene oxide sheets-gold nanoparticles modified electrode. *J. Nanosci. Nanotechnol*. 17, 8012 **(2017)**.
32. X. Z. Zhou, X. Huang, X. Y. Qi, S. X. Wu, C. Xue, F. Y. C. Boey, Q. Y. Yan, P. Chen, and H. Zhang, *In situ* synthesis of metal nanoparticles on single-layer graphene oxide and reduced graphene oxide surfaces. *J. Phys. Chem.* 113, 10842 **(2009)**.
33. C. H. Liu, X. Q. Li, X. P. Jiang, M. Y. Zhuang, J. X. Zhang, C. H. Bao, and Y. W. Zhang, Preparation of functionalized graphene oxide nanocomposites for covalent immobilization of NADH oxidase. *Nanosci. Nanotechnol. Lett.* 8, 164 **(2016)**.
34. S. J. Huang, S. P. Chang, R. W. Chuang, J. T. Lai, Y. K. Su, C. Y. Liu, Z. H. Wang, J. L. Ruan, and C. C. Lin, GaN submicron rods on graphene for nonenzymatic amperometric sensing of glucose. *Nanosci. Nanotechnol. Lett.* 9, 1487 **(2017)**.
35. M. Y. Hua, H. C. Chen, C. K. Chuang, R. Y. Tsai, J. L. Jeng, H. W. Yang, and Y. T. Chern, The intrinsic redox reactions of polyamic acid derivatives and their application in hydrogen peroxide sensor. *Biomaterials* 32, 4885 **(2011)**.
36. S. H. Li, C. Y. Wu, X. Q. Zhao, H. Jiang, H. Yan, and X. M. Wang, Synergistic antibacterial activity of new isomeric carborane derivatives through combination with nanoscaled titania. *J. Biomed. Nanotechnol*. 9, 393 **(2013)**.
37. X. J. Bo, J. Bai, L. X. Wang, and L. P. Guo, *In situ* growth of copper sulfide anoparticles on ordered mesoporous carbon and their application as nonenzymatic amperometric sensor of hydrogen peroxide. *Talanta* 81, 339 **(2010)**.
38. L. An, P. P. Zhou, J. Yin, H. Liu, F. J. Chen, H. Y. Liu, and P. X. Xi, Phase transformation fabrication of a Cu_2S nanoplate as an efficient catalyst for water oxidation with glycine. *Inorg. Chem*. 54, 3281 **(2015)**.
39. Z. Kang, X. Q. Yan, Y. Zhang, J. Pan, J. Shi, X. H. Zhang, Y. Liu, J. H. Choi, and D. M. Porterfield, single-stranded DNA functionalized single-walled carbon nanotubes for microbiosensors via layer-by-layer electrostatic self-assembly. *ACS Appl. Mater. Interfaces* 6, 3784 **(2014)**.

40. X. Y. Chen, H. C. Guo, T. Wang, M. Lu, and T. H. Wang, *In-situ* fabrication of reduced graphene oxide (rGO)/ZnO heterostructure: Surface functional groups induced electrical properties. *Electrochim. Acta* 196, 558 **(2016)**.

41. F. X. Hu, S. H. Chen, C. Y. Wang, R. Yuan, D. H. Yuan, and C. Wang, Study on the application of reduced graphene oxide and multiwall carbon nanotubes hybrid materials for simultaneous determination of catechol, hydroquinone, p-cresol and nitrite. *Anal. Chim. Acta* 724, 40 **(2012)**.

42. D. Z. Wu, X. M. Fan, T. Ke, D. Jia, and H. R. Liu, Fabrication and photocatalytic properties of Cu_2S/T-ZnOw heterostructures via simple polyol process. *Trans. Nonferrous Met. Soc. China* 22, 1620 **(2012)**.

43. Y. G. Zhang, X. M. Li, W. W. Xu, S. Li, H. Z. Wang, and L. Li, The size controlled synthesis and self-assembled of monodisperse Cu_2S nanocrystals. *Mater. Lett*. 67, 117 **(2012)**.

44. N. E. Motl, J. F. Bondi, and R. E. Schaak, Synthesis of colloidal Au–Cu_2S heterodimers via chemically triggered phase segregation of AuCu nanoparticles. *Chem. Mater*. 24, 1552 **(2012)**.

45. Y. Liu, Y. H. Deng, Z. K. Sun, J. Wei, G. F. Zheng, A. M. Asiri, S. B. Khan, M. M. Rahman, and D. Y. Zhao, Hierarchical Cu_2S microsponges constructed from nanosheets for efficient photocatalysis. *Small* 9, 2702 **(2013)**.

46. M. H. Fan, R. Gao, Y. C. Zou, D. J. Wang, N. Bai, G. D. Li, and X. X. Zou, An efficient nanostructured copper(I) sulfide-based hydrogen evolution electrocatalyst at neutral pH. *Electrochim. Acta* 215, 366 **(2016)**.

47. V. H. V. Quy, J. H. Kim, S. H. Kang, C. J. Choi, J. A. Rajesh, and K. S. Ahn, Enhanced electrocatalytic activity of electrodeposited F-doped SnO_2/Cu_2S electrodes for quantum dot-sensitized solar cells. *J. Power Sources* 316, 53 **(2016)**.

48. W. Zhang, L. L. Zhai, N. He, C. Zou, X. Z. Geng, L. J. Cheng, Y. Q. Dong, and S. M. Huang, Solution-based synthesis of wurtzite Cu_2ZnSnS_4 nanoleaves introduced by α-Cu_2S nanocrystals as a catalyst. *Nanoscale* 5, 8114 **(2013)**.

49. A. Khan, A. A. P. Khan, A. M. Asiri, M. A. Rub, M. M. Rahman, and S. A. Ghani, *In vitro* studies of carbon fiber microbiosensor for dopamine neurotransmitter supported by copper-graphene oxide composite. *Microchim. Acta* 181, 1049 **(2013)**.

50. R. L. McCreery, Advanced carbon electrode materials for molecular electrochemistry. *Chem. Rev*. 108, 2646 **(2008)**.

51. C. Yang, C. B. Jacobs, M. D. Nguyen, M. Ganesana, A. G. Zestos, I. N. Ivanov, A. A. Puretzjy, C. M. Rouleau, and B. J. Venton, Carbon nanotubes grown on metal microelectrodes for the detection of dopamine. *Anal. Chem*. 88, 645 **(2015)**.

52. D. L. Robinson, B. J. Venton, M. L. Heien, and R. M. Wightman, Detecting subsecond dopamine release with fast-scan cyclic voltammetry *in vivo*. *Clin. Chem*. 49, 1763 **(2003)**.

53. Q. G. Zhu, J. Ma, X. C. Kang, X. F. Sun, J. Y. Hu, G. Y. Yang, and B. X. Han, Electrochemical reduction of CO_2 to CO using grapheme oxide/carbon nanotube electrode in ionic liquid/acetonitrile system. *Sci. China Chem.* 59, 551 **(2016)**.

54. Y. Deng, W. Wang, L. M. Zhang, Z. X. Lu, S. Li, and L. J. Xu, Preparation and electrochemical behacior of L-glutamate electrochemical biosensor. *J. Biomed. Nanotechnol*. 9, 318 **(2013)**.

55. M. K. Zachek, P. Takmakov, J. Park, R. M. Wightman, and G. S. McCarty, Simultaneous monitoring of dopamine concentration at spatially different brain locations *in vivo*. *Biosens. Bioelectron*. 25, 1179 **(2010)**.

56. T. L. Vickrey, N. Xiao, and B. J. Venton, Kinetics of the dopamine transporter in drosophila larva. *ACS Chem. Neurosci*. 4, 832 **(2013)**.